Bone Reports 4 (2016) 28–34

Contents lists available at ScienceDirect

Bone Reports

journal homepage: www.elsevier.com/locate/bonr

Organ and tissue level properties are more sensitive to age than osteocyte lacunar characteristics in rat cortical bone

Nina Kølln Wittig [a,1], Fiona Linnea Bach-Gansmo [a,1], Mie Elholm Birkbak [a], Malene Laugesen [a], Annemarie Brüel [b], Jesper Skovhus Thomsen [b], Henrik Birkedal [a,*]

[a] iNANO and Department of Chemistry, Aarhus University, Gustav Wieds Vej 14, 8000 Aarhus C, Denmark
[b] Department of Biomedicine, Aarhus University, Aarhus, Denmark

ARTICLE INFO

Article history:
Received 20 November 2015
Accepted 30 November 2015
Available online 2 December 2015

Keywords:
Cortical bone
Mechanical properties
Mineral density
Osteocytes
synchrotron μCT
Aging

ABSTRACT

Modeling and remodeling induce significant changes of bone structure and mechanical properties with age. Therefore, it is important to gain knowledge of the processes taking place in bone over time. The rat is a widely used animal model, where much data has been accumulated on age-related changes of bone on the organ and tissue level, whereas features on the nano- and micrometer scale are much less explored. We investigated the age-related development of organ and tissue level bone properties such as bone volume, bone mineral density, and load to fracture and correlated these with osteocyte lacunar properties in rat cortical bone. Femora of 14 to 42-week-old female Wistar rats were investigated using multiple complementary techniques including X-ray micro-computed tomography and biomechanical testing. The body weight, femoral length, aBMD, load to fracture, tissue volume, bone volume, and tissue density were found to increase rapidly with age at 14–30 weeks. At the age of 30–42 weeks, the growth rate appeared to decrease. However, no accompanying changes were found in osteocyte lacunar properties such as lacunar volume, ellipsoidal radii, lacunar stretch, lacunar oblateness, or lacunar orientation with animal age. Hence, the evolution of organ and tissue level properties with age in rat cortical bone is not accompanied by related changes in osteocyte lacunar properties. This suggests that bone microstructure and bone matrix material properties and not the geometric properties of the osteocyte lacunar network are main determinants of the properties of the bone on larger length scales.

1. Introduction

The skeleton serves vital functions such as support for movement, organ protection, and as a calcium- and phosphate reservoir (Copp and Shim, 1963). Due to modeling and remodeling (Seeman, 2009), the structure and mechanical properties of bone change substantially with age (Mosekilde, 2000). For instance, a common problem for senescent individuals is reduced bone mass, bone mineral density (BMD) and increased risk of osteoporotic fractures and mortality (Johnell and Kanis, 2006). Hence, it is important to study how bone changes as a function of age.

The rat is a widely used animal model in studies of bone, and different aspects of how aging affects structural and mechanical properties of rat cortical bone on the organ (whole/significant part of bone, Fig. 1A) and tissue (Fig. 1B) level have been studied (Akkus et al., 2004; Bak and Andreassen, 1989; Danielsen et al., 1992, 1993; Fukada and Iida, 2004; Hoyer and Lippert, 1982; Iida and Fukuda, 2002; Jast and Jasiuk, 2013; Kiebzak et al., 1988; Nnakwe, 1995; Sontag, 1992; Takee et al., 2002; Vogel, 1979; Wronski et al., 1989; Zhang et al., 2015). Generally, the body weight (Danielsen et al., 1992, 1993; Fukada and Iida, 2004; Hoyer and Lippert, 1982; Iida and Fukuda, 2002; Jast and Jasiuk, 2013; Kiebzak et al., 1988; Nnakwe, 1995; Sontag, 1992), BMD (Danielsen et al., 1993; Fukada and Iida, 2004; Iida and Fukuda, 2002; Zhang et al., 2015), and load to fracture (Akkus et al., 2004; Bak and Andreassen, 1989; Danielsen et al., 1993; Hoyer and Lippert, 1982; Kiebzak et al., 1988; Takee et al., 2002; Vogel, 1979; Zhang et al., 2015; Bone Health and Osteoporosis, 2004) increase with age in the rat. However, discrepencies exist in the literature. For instance, Zhang et al. (2015) and Iida and Fukuda (2002) observed a decrease in BMD in male rat femora initiated at the age of 9 months and 18 months, respectively, and Akkus et al. (2004) observed a decrease in load to fracture in female rat femora from the age of 12 to 24 months.

It is becoming increasingly clear, that the micro- and nanostructural properties of bone are central in determining the quality (Felsenberg and Boonen, 2005) and performance of bone on the macroscale (Dunlop and Fratzl, 2010; Zimmermann and Ritchie, 2015; Tai et al., 2007), and studies employing techniques with high spatial resolution of bone are becoming more frequent (Hesse et al., 2015; Langer et al.,

* Corresponding Author.
E-mail address: hbirkedal@chem.au.dk (H. Birkedal).
[1] These authors contributed equally to the present work.

http://dx.doi.org/10.1016/j.bonr.2015.11.003

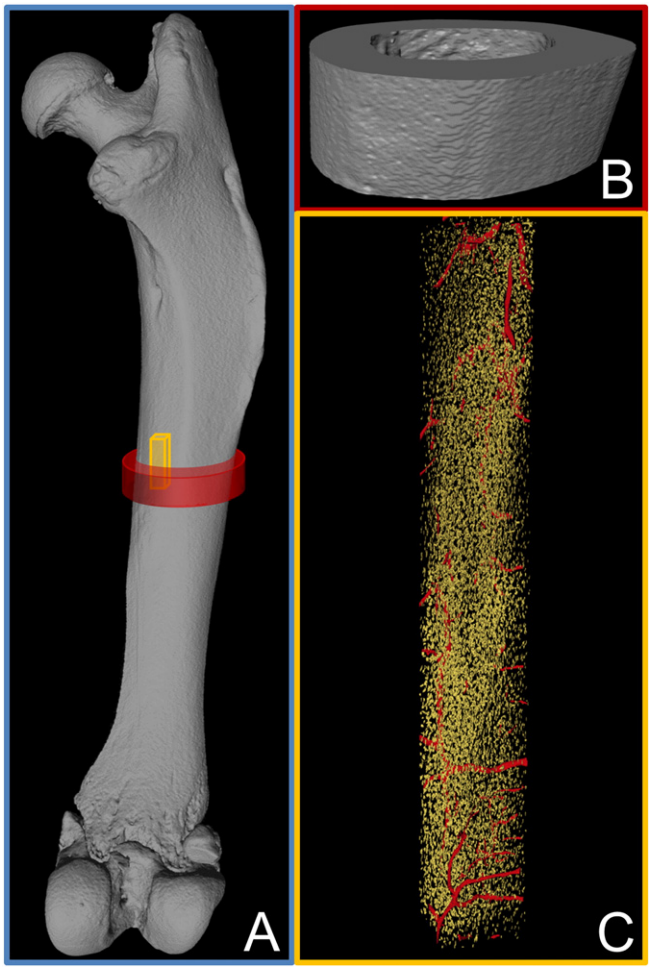

Fig. 1. Length scales investigated in this study range from A the whole bone (blue box) to B the tissue level (red box) and C the material level (yellow box). All images are renderings of μCT data, the whole bone and tissue level from desktop μCT and the material level from synchrotron μCT. In the latter, the internal void space is shown with blood vessel canals in red and osteocyte lacunae in yellow. In the blue box, red and yellow boxes indicate the measured volumes at the tissue and material level, respectively.

2012; Mader et al., 2013; Schneider et al., 2010). Hence, studies that correlate structural and mechanical properties of bone over several length scales are needed in order to better understand age-related changes.

Osteocytes orchestrate bone remodeling and act as mechanotransducers, but an increased understanding of how osteocytes and their activities influence the properties of bone at the tissue level is still needed (Bonewald, 2011; Klein-Nulend et al., 1995; Robling et al., 2008; Skerry et al., 1989; Tatsumi et al., 2007). Considering the large extent of the osteocyte lacunar–canalicular network (LCN) (Schneider et al., 2010), a change in osteocyte lacunar geometry or number could have a significant impact on e.g. the quality and mechanical properties of the whole bone.

The effect of age on osteocyte lacunar characteristics has predominantly been studied in humans and results have been contradictory. Carter et al. reported a decrease in osteocyte lacunar volume (Lc.V) and radii along with a change in lacunar shape, but found no change in osteocyte lacunar orientations or densities with age in women (Carter et al., 2013). However, other studies found the osteocyte lacunar density (Lc.D) to decrease with age (Busse et al., 2010; Mullender et al., 1996). Busse et al. reported an increased amount of hypermineralized calcium phosphate occlusions in osteocyte lacunae with age (Busse et al., 2010). This finding combined with the decrease in Lc.D with age was suggested to be a consequence of osteocytic apoptosis, possibly contributing to failure or delayed bone repair in aged bone. In contrast, Mullender et al. did not find an increased occurrence of osteocytic apoptosis with age (Mullender et al., 1996).

Despite the well established nature and widespread use of rat bone as a model for macrostructural bone studies, few studies have examined rat bone at the sub-100 μm scale. Rat cortical bone is not subjected to Haversian remodeling under normal conditions (Bentolila et al., 1998; Currey, 2002). Thus, the rat provides an excellent opportunity to study the effect of age on bone properties without the interference of Haversian remodeling. Rat femoral cortical bone consists of a central bone zone surrounded by circumferential lamellar bone on the endosteal and periosteal surfaces (Danielsen et al., 1993; Sontag, 1986). With age, the proportion of the two bone zones changes, with central bone being replaced by lamellar bone through combined periosteal apposition and endosteal resorption (Sontag, 1986, 1992). We have previously showed that there are marked differences between central and lamellar bone in rat cortical bone with regard to bone ultrastructure and osteocyte lacunar properties (Bach-Gansmo et al., 2013, 2015). The degree of bone mineralization has also been reported to differ between the two bone zones (Shipov et al., 2013).

The aim of this study is to link the evolution of bone with age across length scales ranging from the material to the organ level (Fig. 1) to test whether there is a coupled age-dependence of the osteocyte lacunar geometry or number and e.g. the quality and mechanical properties of the whole bone. We herein investigate the age development of rat cortical bone using multiple complementary techniques including X-ray micro computed tomography (μCT) at two distinct length scales and biomechanical testing. At the organ level (Fig. 1A) we determine the body weight, femoral length, and areal bone mineral density (aBMD). At the tissue level (Fig. 1B) we determine the mid-diaphyseal load to fracture (F_{max}), tissue volume (TV), bone volume (BV), marrow volume (MV), and tissue density (ρ_{tiss}). At the material level (Fig. 1C) high resolution synchrotron radiation μCT (SR μCT) data is used to determine different osteocyte lacunar properties as well as the local degree of mineralization, the material density (ρ_{mat}). The difference between ρ_{mat} and ρ_{tiss} stems from the length scale over which they are measured: ρ_{mat} will be a measure of the material density excluding osteocyte lacunae and blood vessels while ρ_{tiss} is a value obtained at a larger length scale thus averaging over lacunae and the smallest vessels. To the best of our knowledge, it is the first study to correlate this many parameters covering such a large span in length scales and animal ages.

2. Materials and methods

2.1. Animals and sample preparation

Forty-two 13-week-old female Wistar rats were randomized according to weight into 6 groups ($N = 7$). The rats received an injection of saline into the investigated right hind limb at 14 weeks, as the animals were used as control animals in a different study. The animals were weighed weekly. The animals were sacrificed 0, 4, 8, 12, 16, or 28 weeks after study start, i.e. at ages from 14 to 42 weeks. The right femora were dissected free, cleaned, and the length of the femora was measured using a digital caliper. The femora were frozen in Ringer's solution at −20 °C until further used. The experiment complied with the EU Directive 2010/63/EU for animal experiments, and was approved by the Danish Animal Experiments Inspectorate.

2.2. Dual-energy X-ray absorptiometry (DEXA)

The femora were DEXA scanned (Sabre XL, Norland Stratec, Pforzheim, Germany) using a pixel size of 0.5 mm × 0.5 mm. The areal Bone Mineral Density (aBMD) of the entire femora was determined using the scanner software. Quality assurance was performed by scans of the two solid-state phantoms provided with the scanner. The

coefficient of variation (CV) of rat femoral aBMD is 2.8% in our laboratory (Thomsen et al., 2012).

2.3. Standard desktop micro computed tomography (μCT)

The mid-diaphysis of the femora was investigated with standard desktop μCT (Scanco CT 35, Scanco Medical AG, Brüttisellen, Switzerland). Data was acquired with an X-ray tube operated at 70 kVp, an X-ray current of 114 μA, and a voxel size of $12 \times 12 \times 12\ \mu m^3$. 500 projections/180° were measured with an integration time of 300 ms. The resulting images were low-pass filtered using a Gaussian filter ($\sigma = 0.8$, support = 1) and binarized with a fixed threshold filter (598.9 mg HA/cm^3). Selected cortical bone properties were calculated using IPL (version 5.11, Scanco Medical AG, Brüttisellen, Switzerland).

2.4. Mechanical testing

The femora were subjected to three-point bending test using a materials-testing machine (5566, Instron, High Wycombe, UK) at a deflection rate of 2 mm/min. The load deflection data were measured and recorded with Merlin (version 3.21, Instron, High Wycombe, UK), and load to fracture (F_{max}) was determined using custom software written in C.

2.5. Synchrotron radiation micro computed tomography (SR μCT)

After the three-point bending test, the proximal halves of the femora were cut with a diamond blade saw (Accutom-5, cut off wheel M1D08, Struers, Ballerup, DK) into rods from the anterior-medial quadrants only to ensure that possible quadrant to quadrant variations would not affect the data. Samples matching the circular field of view (832 μm) of the SR μCT setup were made by sawing rods with a maximum rectangular base of $0.58 \times 0.58\ mm^2$. In the *z*-direction, i.e. along the bone long axis, the samples were kept as long as possible, typically a little less than half the femur length.

SR μCT data was acquired at the beamline for TOmographic Microscopy and Coherent rAdiology experimenTs (TOMCAT) at the Swiss Light Source (SLS, Paul Scherrer Institute, Villigen, Switzerland) (Stampanoni et al., 2006). Each sample was waxed onto a sample holder with the long axis aligned along the rotation axis. Three contiguous 702-μm-high scans, starting at the mid-diaphyseal fracture site were measured for all rods with an X-ray energy of 18.0 keV and a voxel size of $0.325 \times 0.325 \times 0.325\ \mu m^3$. 1500/180° projections were measured with an exposure time of 200–210 ms. A 5.5 megapixel CMOS camera (pco.edge 5.5, PCO AG, Kelheim, Germany) coupled to an Optique Peter microscope system with a ×20 lens was used to detect the visible light converted with a 20-μm-thick LAG:Ce scintillator. The experiments were performed with the smallest possible distance between sample and detector, hence close to pure absorption contrast was measured. The image reconstructions were made using the GridRec algorithm with a Parzen filter (Marone et al., 2010).

2.6. SR μCT image post processing

The SR μCT data sets were analyzed with the Fiji plugin BoneJ (Schindelin et al., 2012). The image resolution is affected by the precision of the focus. This was found only to be optimal for a subset of the data. For each image stack, the images corresponding to optimal focus conditions, and hence highest resolution, were selected and these data were used for further data analysis. Each image stack of reconstructions was binarized using the Optimize Threshold function. Osteocyte lacunar volume (Lc.V) and best fit ellipsoidal axes were calculated using the Particle Analyzer functionality of Fiji. Volumes below 50 μm^3 were excluded in order to remove noise and canaliculi (which are not fully resolved at the current resolution) from the analysis, and in order to remove blood vessels, volumes above 1500 μm^3 were excluded. In addition, osteocyte lacunae touching the sample surface were excluded from the analysis.

The osteocyte lacunar data were further analyzed using custom written MATLAB code (R2014b, MathWorks, Natick, MA). For each sample, data from the three image stacks were combined. The osteocyte lacunar density (Lc.D), orientation (Lc.Or), and shape were calculated. Lc.D was evaluated as the number of osteocyte lacunae per mm^3 volume of sample. Lc.Or was characterized relative to the *z*-axis (the bone long axis) and relative to the *x*-axis for the in-plane orientation. This was obtained as the angle between the longest best fit ellipsoidal axis and the *z*-axis and the angle between the *x*-axis and the projection of the longest best fit ellipsoid on the *xy*-plane, respectively (Bach-Gansmo et al., 2015). This provided a set of angles from which the average angle and the angle distribution were calculated; the latter by computing a histogram. The distribution was characterized by its entropy that was calculated as described by Bach-Gansmo et al. (2015) using the formula $S = \sum_{i=1}^{N} p_i \ln p_i$, with p_i being the value of the frequency in the distribution that was sampled in *N* bins (Rich and Tracy, 2010). The entropy is small for a peaked distribution and large for a flat one and is dependent on sampling density. The in-plane orientation is only discussed through the entropy because the sample absolute in-plane orientation was not determined. The osteocyte lacunar shape was described by lacunar stretch ($Lc.St = \frac{r_3 - r_1}{r_3}$) and lacunar oblateness ($Lc.Ob = 2 \cdot \frac{r_2 - r_1}{r_3 - r_1} - 1$) (Mader et al., 2013), using the best fit ellipsoidal radii ($r_1 < r_2 < r_3$). Histograms of the above mentioned properties were all normalized according to the total number of lacunae in the respective animal, and age-averaged histograms were then computed from these individual histograms. The bin size was adapted to each individual property.

The bone material density (ρ_{mat}) of the samples was evaluated based on the original reconstruction images using custom written MATLAB code. For each femur, a gray level histogram was constructed from 200 images selected from each image stack comprising 600 images per femur. The gray level corresponding to the bone mineral peak was extracted and the average values analyzed as a function of age. Since data were measured in almost pure absorption contrast mode, the gray levels of the images are measures of the mineral density. We report as gray levels herein since this work focuses on relative age-related changes.

2.7. Statistical analysis

Statistical comparisons were made using ANOVA and the Tukey–Kramer method with normality assured by the Lilliefors test. Differences were considered significant at $p < 0.05$. The statistical analysis of osteocyte lacunar properties were implemented in MATLAB (R2014b, MathWorks, Natick, MA), while the analysis of all other properties was done in Origin (version 8.0, OriginLab, Northampton, MA). Values are, unless specified otherwise, reported as mean ± SD, were SD is the standard deviation. Pearson correlation coefficients were also evaluated using custom software written in C providing a measure of the linear correlation between all properties (Pearson, 1896).

3. Results

The age-related changes of selected organ and tissue level properties are reported in Fig. 2. Fig. 2A–D reveals that the average body weight, femoral length, aBMD, and diaphyseal F_{max} increase significantly with increasing age. As the rats mature the growth levels off. The μCT data are presented in Fig. 2E–H. The average tissue volume (TV), bone volume (BV), and tissue density (ρ_{tiss}) show a similar increase with age. Statistical comparisons (ANOVA) reveal a significant difference between the age groups for the average body weight ($p < 0.001$), femoral length ($p < 0.001$), aBMD ($p < 0.001$), F_{max} ($p < 0.001$), TV ($p < 0.001$), BV ($p < 0.001$), and ρ_{tiss} ($p < 0.001$). Use of the Tukey–Kramer method confirmed that the properties increased continually with age. No trend is

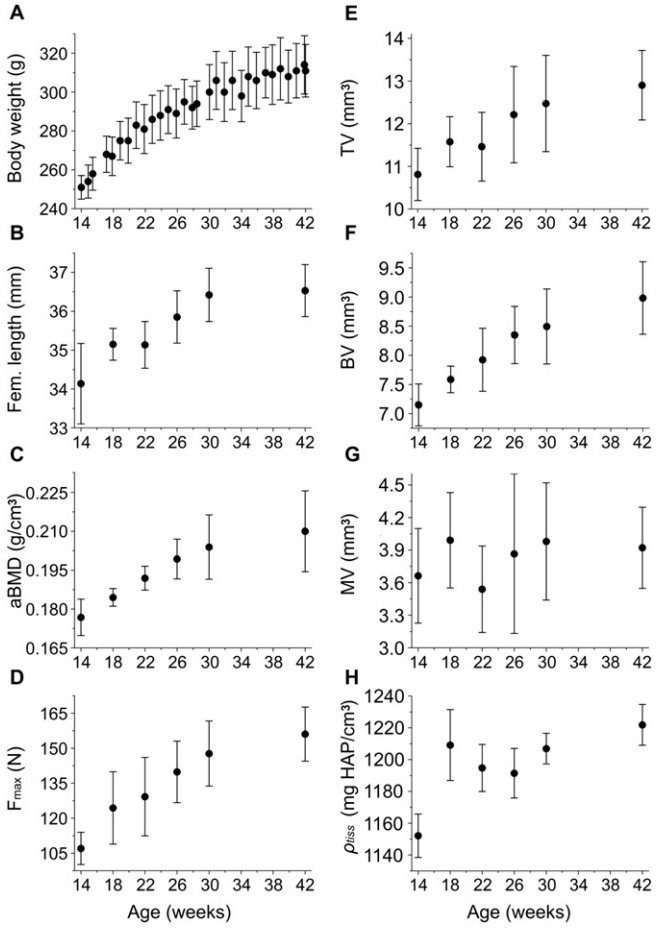

Fig. 2. Age development of the average A body weight, B femoral length, C aBMD as measured by DEXA, D mid-diaphyseal load to fracture (F_{max}), E mid-diaphyseal tissue volume (TV), F mid-diaphyseal bone volume (BV), G mid-diaphyseal marrow volume (MV), and H mid-diaphyseal tissue density (ρ_{tiss}). Note that the second axes do not originate in zero.

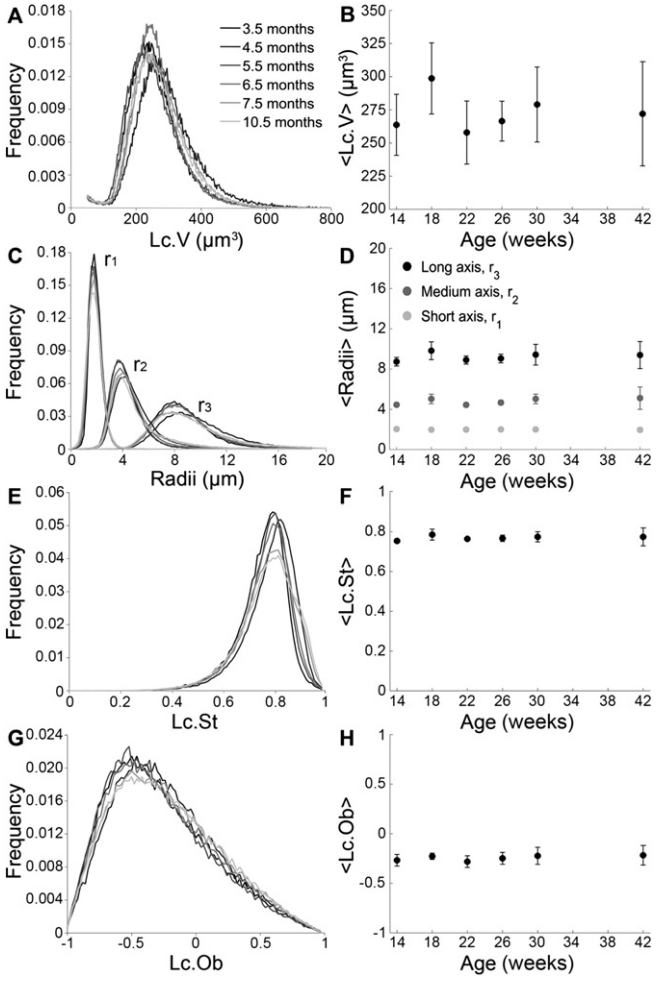

Fig. 3. SR μCT data showing A the lacunar volume (Lc.V) distribution, B the average Lc.V as a function of age, C the best fit ellipsoidal radii distribution, D the average ellipsoidal radii as a function of age, E the lacunar stretch (Lc.St) distribution, F the average Lc.St as a function of age, G the osteocyte lacunar oblateness (Lc.Ob) distribution, and H the average Lc.Ob as a function of age. All distributions are normalized according to the total number of osteocyte lacunae in the respective age group. The distributions are gray scale coded according to age, with increasing gray level values with increasing age.

apparent for the average marrow volume (MV) with age (Fig. 2G), and no significant differences are detected.

Osteocyte lacunar properties obtained from synchrotron radiation μCT are presented in Fig. 3. The left hand column (Fig. 3A, C, E, G) reports average distributions of relevant quantities obtained by averaging the histograms from each individual animal. The right hand column displays the age dependence of the average values (Fig. 3B, D, F, H). The Lc.V distributions and their averages, <Lc.V>, are presented as a function of age in Fig. 3A and B. The different age-groups do not differ significantly from each other. The global average value of <Lc.V> taken over all individuals and age groups is $273 \pm 29\ \mu m^3$. The ellipsoidal radii exhibit log-normal distributions (Fig. 3C) with well-defined ranges of the shortest (r_1) to the longest (r_3) radius. The average radii for the different age-groups do not differ from each other (Fig. 3D). Dimensions of $<r_1> = 2.0 \pm 0.1\ \mu m$, $<r_2> = 4.8 \pm 0.6\ \mu m$, and $<r_3> = 9.2 \pm 0.9\ \mu m$ are obtained when averaging over all individuals and age groups. The distribution of r_3 appears wider (Fig. 3C), but evaluation of the relative average width (full width half maximum/average radius) reveal that the relative spread of the shortest axis is in fact the largest ($p < 0.05$). The Lc.St distribution and average as a function of age is shown in Fig. 3E and F, and the age-groups again do not differ from each other. The Lc.Ob distribution (Fig. 3G) and average (Fig. 3H) reveal no significant differences between the age-groups. The global averages over all individuals and age groups are $<Lc.St> = 0.77 \pm 0.03$ and $<Lc.Ob> = -0.24 \pm 0.07$, respectively.

The orientation of the long lacunar axis is presented in Fig. 4. The orientation with respect to the bone long axis is presented as a function

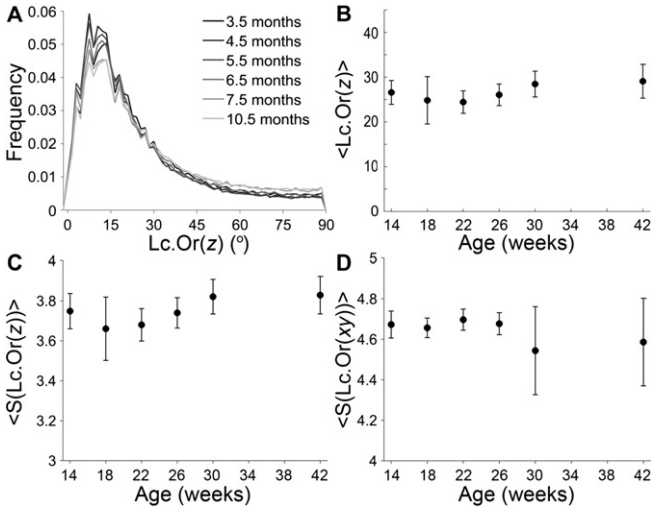

Fig. 4. SR μCT data showing lacunar orientation (Lc.Or) as a function of age. The Lc.Or with respect to the bone long axis (z-axis) is presented as A the distribution, B the average, and C the average entropy of the distribution. The Lc.Or in the xy-plane is presented in D as the average entropy of the distribution.

of age with distributions (Fig. 4A), average values (Fig. 4B) and average entropy of the distributions (Fig. 4C), revealing no differences between age groups. Averaging over all individuals and age groups gives $<Lc.Or(z)> = 27 \pm 4°$ and $<S(Lc.Or(z))> = 3.7 \pm 0.1$. The orientation in the *xy*-plane is presented as the average entropy of the distributions, Fig. 4D. No differences are observed between age groups, and an average over all age groups of $<S(Lc.Or(xy))> = 4.6 \pm 0.1$ is obtained. Note the larger standard deviation for the orientation in the *xy*-plane in the 30 and 42 weeks age groups. In each of these groups, a single outlier was detected. Closer investigation of the corresponding reconstructions revealed a high amount of lamellar bone in these scans compared to the other samples.

The distributions are normalized according to the total number of lacunae in the respective age group. The distributions are color coded according to age, with increasing gray level values with increasing age.

The average Lc.D and mineral density are shown in Fig. 5 as a function of age. The Lc.D of the 30-week-old rats differs significantly from the 14- and 22-week-old rats ($p < 0.05$) (Fig. 5A) but no other significant differences could be detected. The average material density (ρ_{mat}) reported in gray level (Fig. 5B) increases continually with age ($p < 0.05$).

Pearson correlation coefficients with *p*-values below the significance level of 0.05 are displayed in Table 1 for the organ and tissue level properties and selected osteocyte lacunar characteristics. In agreement with the results presented in Figs. 2–4, strong positive correlations are generally found between age and the organ and tissue level properties, while age is not correlated to the osteocyte lacunar characteristics. A negative correlation exists between age and the Lc.D ($r = -0.41$, $p < 0.01$) and a strong positive correlation is found between age and the ρ_{mat} ($r = 0.80$, $p < 0.01$) as was also observed in Fig. 5.B. The body weight and age are highly correlated ($r = 0.81$, $p < 0.01$), and the correlations of all other properties to the body weight and age, respectively, are similar. In general, high positive correlations are observed among all organ and tissue level properties with the exception of MV that is not correlated to body weight, aBMD or ρ_{tiss}, and only slightly correlated to age ($r = 0.15$, $p < 0.05$) and femoral length ($r = 0.34$, $p < 0.05$).

4. Discussion

In the present study we found that the structural and mechanical parameters on the organ and tissue level of rat cortical bone depend on animal age, with the exception of MV. The average body weight, femoral length, aBMD, F_{max}, TV, BV, and ρ_{tiss} increase rapidly with age in the beginning of the experiment (i.e. for younger rats), while the growth rate appears to decrease at the end of the experiment (i.e. at the age of 30–42 weeks). This indicates that the rats have not completed their rapid growth period before this stage, in agreement with previous findings (Danielsen et al., 1993; Fukada and Iida, 2004; Hoyer and Lippert, 1982; Jast and Jasiuk, 2013; Kiebzak et al., 1988; Nnakwe, 1995; Sontag, 1992; Takee et al., 2002; Wronski et al., 1989), except a few studies showing a constant BV from three months and onwards in tibia from female Sprague–Dawley rats (Jast and Jasiuk, 2013; Wronski et al., 1989). In general, growth plates in rat long bones remain open throughout most of the rat's lifespan (Sontag, 1992; Wronski et al., 1989). However, it is widely accepted that rats are sexually mature already after six weeks implicating that e.g. hormone levels, which affect the activity of bone cells are stable from here on (Sengupta, 2013). Overall, it is important to take both sexual maturity and state of growth into consideration when studying bone, and equally important when making comparisons between studies.

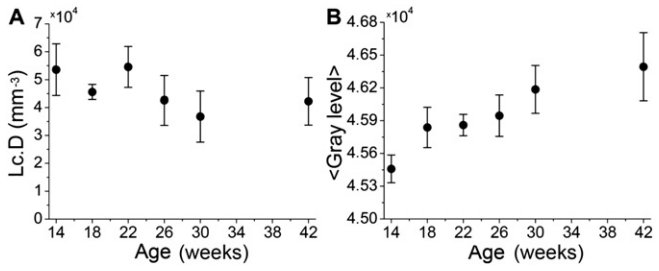

Fig. 5. SR-μCT data showing A the average lacunar density (Lc.D) as a function of age, and B the average material density (ρ_{mat}) obtained as the gray level values as a function of age.

Pearson correlation analysis showed strong positive correlation between many parameters on the organ and tissue level. As expected, age and body weight were strongly correlated. Indeed, previous studies have even used the weight of wild animals as an estimate of their age (Dawson, 1934). Correspondingly, it is not surprising that the organ and tissue level properties are correlated to the age and average body weight to a similar degree. Strong correlations are observed between the average BV, aBMD, and F_{max} at the femoral mid-diaphysis, in agreement with previous results implicating higher strength in larger, more highly mineralized bone (Follet et al., 2004; Milovanovic et al., 2015; Yao et al., 2007). However, BV and F_{max} exhibit lower correlation coefficients to the average ρ_{tiss} and ρ_{mat} than to the aBMD. Whereas ρ_{tiss} and ρ_{mat} are local measures of the mineral density at the tissue and material length scales, respectively, aBMD is an average value of the entire femur including void space and suffering from reporting an areal density rather than a volumetric density (Koller and Laib, 2007).

Since osteocytes orchestrate bone remodeling and act as mechanotransducers, one could be prone to hypothesize that changes on the organ and tissue level would be accompanied by or preceded by changes in the LCN. However, our high resolution studies of osteocyte lacunar geometries revealed no significant changes in Lc.V, ellipsoidal radii, Lc.St, Lc.Ob, or Lc.Or with animal age, despite the changes observed on the organ and tissue level. The same is seen in the Pearson correlation analysis, where the only geometric property that shows a small but significant correlation to age is S(Lc.Or(z)).

Previous reports on age-related changes of osteocyte lacunar volumes and ellipsoidal radii have been contradictory. A significant decrease in Lc.V as a result of decreasing radii with age was reported in female human femora (Carter et al., 2013), while no differences were found for Lc.V or lacunar length in tibia of female Sprague–Dawley rats (Jast and Jasiuk, 2013). Mineral occlusions in osteocyte lacunae and the ability of osteocytes to form mineral, has previously been suggested to explain reduced osteocyte lacunar size with age (Carter et al., 2013; Busse et al., 2010; Frost, 1960). Bone formation by osteocytes was observed in femoral diaphysis of male Sprague–Dawley rats aged 31–48 days using labeling with tetracycline (Baylink and Wergedal, 1971).

In the present study, we employed very high resolution ($0.325 \times 0.325 \times 0.325\ \mu m^3$ voxel size) and measured no less than $7.4 \cdot 10^5$ osteocyte lacunae. However, these high quality data did not reveal any changes in Lc.V, despite the significant changes in aBMD, ρ_{tiss}, and ρ_{mat} with age in rats. Hence, removal and/or deposition of mineral by osteocytes with age, does not occur to such an extent that it is detectable as changes in Lc.V or radii in the present setup.

The shape of the osteocyte lacunae was investigated from best fit ellipsoids in agreement with generally accepted practice (Mader et al., 2013; Carter et al., 2014; Dong et al., 2014; Marotti, 1979; McCreadie and Hollister, 1997; McCreadie et al., 2004). The shape of the osteocyte lacunae is likely important for strain concentration and mechanosensing properties of the osteocytes (McCreadie and Hollister, 1997; McCreadie et al., 2004; van Oers et al., 2015). To the best of our knowledge, the present study is the first to investigate osteocyte lacunar shape as a function of age in rats. No significant changes were found in Lc.St or Lc.Ob with age, indicating that the changes observed on the organ and tissue level occurred independently of lacunar shape. Similarly, McCreadie et al. found no differences in lacunar size and shape between healthy and osteoporotic women (McCreadie et al., 2004). On the other hand, Van Hove et al. did find significant differences in lacunar shape between human tibial bone of differing bone mineral density, with more round osteocytes in osteopenic bone compared to osteoarthritic

Table 1
Pearson correlation coefficients for organ and tissue level properties and selected osteocyte lacunar characteristics. Coefficients with a p-value above the significance level of 0.05 are not shown. Coefficients with $p < 0.01$ are marked in bold.

	Body weight	Fem. length	aBMD	F_{max}	TV	BV	MV	ρ_{tiss}	ρ_{mat}	Lc.D	Lc.V	Lc.St	Lc.Ob	S(Lc.Or(z))	S(Lc.Or(xy))
Age	**0.81**	**0.71**	**0.75**	**0.75**	**0.62**	**0.77**	0.15	**0.62**	**0.80**	**−0.41**				0.39	
Body weight		**0.82**	**0.80**	**0.75**	**0.67**	**0.77**		**0.46**	**0.62**	−0.34					
Fem. length			**0.74**	**0.73**	**0.67**	**0.71**	0.34	**0.53**	**0.63**	**−0.40**					
aBMD				**0.84**	**0.75**	**0.89**		**0.45**	**0.55**	−0.37					
F_{max}					**0.87**	**0.92**	**0.46**	**0.46**	**0.61**	**−0.42**					
TV						**0.91**	**0.76**		**0.42**	**−0.41**			0.32		−0.31
BV							**0.42**	**0.45**	**0.56**	**−0.41**					
MV															
ρ_{tiss}									**0.72**						
ρ_{mat}										**−0.48**		**0.43**	0.38	0.38	**−0.42**
Lc.D													**−0.62**	**−0.54**	**0.70**
Lc.V												**0.74**			
Lc.St													0.37		
Lc.Ob														**0.60**	**−0.81**
S(Lc.Or(z))															**−0.64**

The three measures of mineralization density, aBMD, ρ_{tiss}, and ρ_{mat} are all inter-correlated with r lying in the range of 0.45–0.72 ($p < 0.01$). The ρ_{mat} is somewhat correlated to the osteocyte lacunar characteristics ($0.43 < |r| < 0.48$) with the exception of Lc.V, while aBMD and ρ_{tiss} are not. Lc.V only correlates to Lc.St ($r = 0.74$, $p < 0.01$). Lc.St. also correlates positively to S(Lc.Or(z)) ($r = 0.60$, $p < 0.01$) and negatively to S(Lc.Or(xy)) ($r = -0.81$, $p < 0.01$). Moreover, S(Lc.Or(xy)) exhibit a positive correlation to Lc.D ($r = 0.70$, $p < 0.01$), negative correlations to Lc.Ob ($r = -0.81$, $p < 0.01$) and S(Lc.Or(z)) ($r = -0.64$, $p < 0.01$), and a low negative correlation to TV ($r = -0.31$, $p < 0.05$).

and osteopetrotic bone (van Hove et al., 2009). A change in lacunar morphology with age was reported in femora of women, with more flat and less equant lacunae in younger women, with equancy defined as r_1/r_3 (Carter et al., 2013). It should be noted that both osteocyte lacunar shape and osteocyte shape are likely to influence the bone cell mechanosensation (van Oers et al., 2015). In vitro studies of MLO-Y4 osteocytes show that round osteocytes are more mechanosensitive than flat osteocytes (Bacabac et al., 2008). Interestingly, we see a significant positive correlation between Lc.St and Lc.V indicating that larger osteocyte lacunae are more elongated than smaller ones.

Lc.Or did not change with age in agreement with previous reports in humans (Carter et al., 2013) and Sprague–Dawley rats (Jast and Jasiuk, 2013). Femora from older rats are expected to contain a higher proportion of lamellar bone than younger rats (Sontag, 1986), and previous results showed that the entropy of the Lc.Or distribution in the *xy*-plane is lower in lamellar bone compared to central bone (Bach-Gansmo et al., 2015). A single outlier containing a high amount of lamellar bone was detected in each of the 30 and 42 weeks age groups. The lower entropy of Lc.Or in the *xy*-plane in these outliers explains the relatively large standard deviation in these groups. Additionally, a negative correlation was found between the entropy of Lc.Or in the *xy*-plane and TV, supporting the fact that lamellar bone is deposited on the periosteal surfaces with age (Sontag, 1986). An increasing amount of lamellar bone with age is further supported by the negative correlation between age and Lc.D, since Lc.D is lower in lamellar bone compared to central bone (Bach-Gansmo et al., 2015). However, the present study did not reveal a clear significantly decreasing trend in Lc.D with age as expected from a higher proportion of lamellar bone. Nevertheless, significant differences in Lc.D between the 30-week-old rats and the 14- and 22-week-old rats were found. Jast and Jasiuk (2013) reported no significant change in Lc.D with age in tibia of female Sprague–Dawley rats, but their data did reveal a trend of decreasing Lc.D. In humans, a decreasing Lc.D with age has been reported in either a non-significant (Carter et al., 2013; Vashishth et al., 2005) or a significant manner (Busse et al., 2010; Mullender et al., 1996). Ma et al. found a positive correlation between osteocyte density and maximum load in vertebrae of female Sprague–Dawley rats (Ma et al., 2008), while a slight negative correlation was found in the present work. However, the difference in site and rat strain between these two studies should be noted. Additionally, it should be stressed that the effect of aging is different when comparing rat and human bone. Where the mineral density and size of bone increase with age in rats, it is the opposite in human bone.

The Pearson correlation analysis shows that generally, the osteocyte lacunar characteristics do not correlate to age or to the organ and tissue level properties. Consequently, the present study show no indications that changes with age on the organ and tissue level are accompanied by or preceded by changes in osteocyte lacunar geometries. However, it cannot be excluded that changes with age occur on the canalicular and pericanalicular level that would be below the detection limit of the present study.

In conclusion, the macrostructure can be altered without changing osteocyte lacunar geometries in rat cortical bone. This indicates that bone microstructure and bone matrix material properties and not the geometric properties of the osteocyte lacunae determine the properties of the bone on larger length scales.

Acknowledgments

We acknowledge the Paul Scherrer Institut, Villigen, Switzerland for provision of synchrotron radiation beamtime at beamline TOMCAT of the SLS and in particular Kevin Mader for assistance with the synchrotron measurements. The research leading to these results has received funding from the European Community's Seventh Framework Programme (FP7/2007-2013) under grant agreement no. 312284 (for CALIPSO). Additional funding from the Danish Agency for Science, Technology and Innovation (DANSCATT) is gratefully acknowledged.

References

Akkus, O., Adar, F., Schaffler, M.B., 2004. Age-related changes in physicochemical properties of mineral crystals are related to impaired mechanical function of cortical bone. Bone 34, 443–453.

Bacabac, R.G., Mizuno, D., Schmidt, C.F., MacKintosh, F.C., Van Loon, J.J., Klein-Nulend, J., Smit, T.H., 2008. Round versus flat: bone cell morphology, elasticity, and mechanosensing. J. Biomech. 41, 1590–1598.

Bach-Gansmo, F.L., Irvine, S.C., Bruel, A., Thomsen, J.S., Birkedal, H., 2013. Calcified cartilage islands in rat cortical bone. Calcif. Tissue Int. 92, 330–338.

Bach-Gansmo, F.L., Weaver, J.C., Jensen, M.H., Leemreize, H., Mader, K.S., Stampanoni, M., Bruel, A., Thomsen, J.S., Birkedal, H., 2015. Osteocyte lacunar properties in rat cortical bone: differences between lamellar and central bone. J. Struct. Biol. 191, 59–67.

Bak, B., Andreassen, T.T., 1989. The effect of aging on fracture healing in the rat. Calcif. Tissue Int. 45, 292–297.

Baylink, D.J., Wergedal, J.E., 1971. Bone formation by osteocytes. Am. J. Physiol. 221, 669–678.

Bentolila, V., Boyce, T.M., Fyhrie, D.P., Drumb, R., Skerry, T.M., Schaffler, M.B., 1998. Intracortical remodeling in adult rat long bones after fatigue loading. Bone 23, 275–281.

Bone Health and Osteoporosis, 2004. A Report of the Surgeon General. In: U.S. Department of Health and Human Services (Ed.)U.S. Department of Health and Human Services OotSGU, Rockville (MD).

Bonewald, L.F., 2011. The amazing osteocyte. J. Bone Miner. Res. 26, 229–238.

Busse, B., Djonic, D., Milovanovic, P., Hahn, M., Puschel, K., Ritchie, R.O., Djuric, M., Amling, M., 2010. Decrease in the osteocyte lacunar density accompanied by

hypermineralized lacunar occlusion reveals failure and delay of remodeling in aged human bone. Aging Cell 9, 1065–1075.
Carter, Y., Thomas, C.D., Clement, J.G., Cooper, D.M., 2013. Femoral osteocyte lacunar density, volume and morphology in women across the lifespan. J. Struct. Biol. 183, 519–526.
Carter, Y., Suchorab, J.L., Thomas, C.D., Clement, J.G., Cooper, D.M., 2014. Normal variation in cortical osteocyte lacunar parameters in healthy young males. J. Anat. 225, 328–336.
Copp, D.H., Shim, S.S., 1963. The homeostatic function of bone as a mineral reservoir. Oral Surg. Oral Med. Oral Pathol. 16, 738–744.
Currey, J., 2002. Bone: Structure and Mechanisms. Princeton University Press, Princeton.
Danielsen, C.C., Mosekilde, L., Andreassen, T.T., 1992. Long-term effect of orchidectomy on cortical bone from rat femur: bone mass and mechanical properties. Calcif. Tissue Int. 50, 169–174.
Danielsen, C.C., Mosekilde, L., Svenstrup, B., 1993. Cortical bone mass, composition, and mechanical properties in female rats in relation to age, long-term ovariectomy, and estrogen substitution. Calcif. Tissue Int. 52, 26–33.
Dawson, A.B., 1934. Additional evidence of the failure of epiphyseal union in the skeleton of the rat studies on wild and captive gray Norway rats. Anat. Rec. 60, 501–511.
Dong, P., Haupert, S., Hesse, B., Langer, M., Gouttenoire, P.J., Bousson, V., Peyrin, F., 2014. 3D osteocyte lacunar morphometric properties and distributions in human femoral cortical bone using synchrotron radiation micro-CT images. Bone 60, 172–185.
Dunlop, J.W.C., Fratzl, P., 2010. Biological composites. Annu. Rev. Mater. Res. Vol. 40, 1–24 (40).
Felsenberg, D., Boonen, S., 2005. The bone quality framework: determinants of bone strength and their interrelationships, and implications for osteoporosis management. Clin. Ther. 27, 1–11.
Follet, H., Boivin, G., Rumelhart, C., Meunier, P.J., 2004. The degree of mineralization is a determinant of bone strength: a study on human calcanei. Bone 34, 783–789.
Frost, H.M., 1960. Micropetrosis. J. Bone Joint Surg. Am. 42-A, 144–150.
Fukada, S., Iida, H., 2004. Age-related changes in bone mineral density, cross-sectional area and the strength of long bones in the hind limb and first lumbar vertebra in female Wistar rats. Lab. Anim. Sci. 66, 755–760.
Hesse, B., Varga, P., Langer, M., Pacureanu, A., Schrof, S., Mannicke, N., Suhonen, H., Maurer, P., Cloetens, P., Peyrin, F., Raum, K., 2015. Canalicular network morphology is the major determinant of the spatial distribution of mass density in human bone tissue: evidence by means of synchrotron radiation phase-contrast nano-CT. J. Bone Miner. Res. 30, 346–356.
Hoyer, H.E., Lippert, H., 1982. Biomechanical changes in long limb bones of Han–Wistar rats during postnatal-development. Anat. Embryol. 164, 101–111.
Iida, H., Fukuda, S., 2002. Age-related changes in bone mineral density, cross-sectional area and strength at different skeletal sites in male rats. J. Vet. Med. Sci. 64, 29–34.
Jast, J., Jasiuk, I., 2013. Age-related changes in the 3D hierarchical structure of rat tibia cortical bone characterized by high-resolution micro-CT. J. Appl. Physiol. 114, 923–933 (1985).
Johnell, O., Kanis, J.A., 2006. An estimate of the worldwide prevalence and disability associated with osteoporotic fractures. Osteoporos. Int. 17, 1726–1733.
Kiebzak, G.M., Smith, R., Howe, J.C., Gundberg, C.M., Sacktor, B., 1988. Bone status of senescent female rats: chemical, morphometric, and biomechanical analyses. J. Bone Miner. Res. 3, 439–446.
Klein-Nulend, J., van der Plas, A., Semeins, C.M., Ajubi, N.E., Frangos, J.A., Nijweide, P.J., Burger, E.H., 1995. Sensitivity of osteocytes to biomechanical stress in vitro. FASEB J. 9, 441–445.
Koller, B., Laib, A., 2007. Calibration of micro-CT data for quantifying bone mineral and biomaterial density and microarchitecture. Advanced Bioimaging Technologies in Assessment of the Quality of Bone and Scaffold Materials: Techniques and Applicationspp. 79–84.
Langer, M., Pacureanu, A., Suhonen, H., Grimal, Q., Cloetens, P., Peyrin, F., 2012. X-ray phase nanotomography resolves the 3D human bone ultrastructure. PLoS One 7, e35691.
Ma, Y.L., Dai, R.C., Sheng, Z.F., Jin, Y., Zhang, Y.H., Fang, L.N., Fan, H.J., Liao, E.Y., 2008. Quantitative associations between osteocyte density and biomechanics, microcrack and microstructure in OVX rats vertebral trabeculae. J. Biomech. 41, 1324–1332.
Mader, K.S., Schneider, P., Muller, R., Stampanoni, M., 2013. A quantitative framework for the 3D characterization of the osteocyte lacunar system. Bone 57, 142–154.
Marone, F., Munch, B., Stampanoni, M., 2010. Fast reconstruction algorithm dealing with tomography artifacts. Developments in X-Ray Tomography VIIp. 7804.
Marotti, G., 1979. Osteocyte orientation in human lamellar bone and its relevance to the morphometry of periosteocytic lacunae. Metab. Bone Dis. Relat. Res. 1, 325–333.
McCreadie, B.R., Hollister, S.J., 1997. Strain concentrations surrounding an ellipsoid model of lacunae and osteocytes. Comput. Methods Biomech. Biomed. Engin. 1, 61–68.
McCreadie, B.R., Hollister, S.J., Schaffler, M.B., Goldstein, S.A., 2004. Osteocyte lacuna size and shape in women with and without osteoporotic fracture. J. Biomech. 37, 563–572.
Milovanovic, P., Zimmermann, E.A., Riedel, C., Scheidt, A.V., Herzog, L., Krause, M., Djonic, D., Djuric, M., Puschel, K., Amling, M., Ritchie, R.O., Busse, B., 2015. Multi-level characterization of human femoral cortices and their underlying osteocyte network reveal trends in quality of young, aged, osteoporotic and antiresorptive-treated bone. Biomaterials 45, 46–55.
Mosekilde, L., 2000. Age-related changes in bone mass, structure, and strength — effects of loading. Zeitschrift Fur Rheumatologie 59, 1–9.
Mullender, M.G., van der Meer, D.D., Huiskes, R., Lips, P., 1996. Osteocyte density changes in aging and osteoporosis. Bone 18, 109–113.
Nnakwe, N.E., 1995. The effect of aging on bone composition of female Fischer 344 rats. Mech. Ageing Dev. 85, 125–131.
Pearson, 1896. Mathematical contributions to the theory of evolution. III. Regression, heredity and panmixia. Philos. Trans. R. Soc. Lond. 187, 253–318.
Rich, R., Tracy, J., 2010. The relationships among expected inflation, disagreement, and uncertainty: evidence from matched point and density forecasts. Rev. Econ. Stat. 92, 200–207.
Robling, A.G., Niziolek, P.J., Baldridge, L.A., Condon, K.W., Allen, M.R., Alam, I., Mantila, S.M., Gluhak-Heinrich, J., Bellido, T.M., Harris, S.E., Turner, C.H., 2008. Mechanical stimulation of bone in vivo reduces osteocyte expression of Sost/sclerostin. J. Biol. Chem. 283, 5866–5875.
Schindelin, J., Arganda-Carreras, I., Frise, E., Kaynig, V., Longair, M., Pietzsch, T., Preibisch, S., Rueden, C., Saalfeld, S., Schmid, B., Tinevez, J.Y., White, D.J., Hartenstein, V., Eliceiri, K., Tomancak, P., Cardona, A., 2012. Fiji: an open-source platform for biological-image analysis. Nat. Methods 9, 676–682.
Schneider, P., Meier, M., Wepf, R., Muller, R., 2010. Towards quantitative 3D imaging of the osteocyte lacuno-canalicular network. Bone 47, 848–858.
Seeman, E., 2009. Bone modeling and remodeling. Crit. Rev. Eukaryot. Gene Expr. 19, 219–233.
Sengupta, P., 2013. The laboratory rat: relating its age with human's. Int. J. Prev. Med. 4, 624–630.
Shipov, A., Zaslansky, P., Riesemeier, H., Segev, G., Atkins, A., Shahar, R., 2013. Unremodeled endochondral bone is a major architectural component of the cortical bone of the rat (Rattus norvegicus). J. Struct. Biol. 183, 132–140.
Skerry, T.M., Bitensky, L., Chayen, J., Lanyon, L.E., 1989. Early strain-related changes in enzyme activity in osteocytes following bone loading in vivo. J. Bone Miner. Res. 4, 783–788.
Sontag, W., 1986. Quantitative measurements of periosteal and cortical-endosteal bone formation and resorption in the midshaft of male rat femur. Bone 7, 63–70.
Sontag, W., 1992. Age-dependent morphometric alterations in the distal femora of male and female rats. Bone 13, 297–310.
Stampanoni, M., Groso, A., Isenegger, A., Mikuljan, G., Chen, Q., Bertrand, A., Henein, S., Betemps, R., Frommherz, U., Bohler, P., Meister, D., Lange, M., Abela, R., 2006. Trends in synchrotron-based tomographic imaging: the SLS experience. Developments in X-ray Tomography Vp. 6318.
Tai, K., Dao, M., Suresh, S., Palazoglu, A., Ortiz, C., 2007. Nanoscale heterogeneity promotes energy dissipation in bone. Nat. Mater. 6, 454–462.
Takee, A., Hirano, J., Uchikura, C., Ohmori, S., Kodera, M., Kotani, A., Ishii, Y., Nakahara, H., 2002. Effects of drug treatment on bone strength and structural changes with aging: an experimental study in rats. J. Orthop. Sci. 7, 544–548.
Tatsumi, S., Ishii, K., Amizuka, N., Li, M., Kobayashi, T., Kohno, K., Ito, M., Takeshita, S., Ikeda, K., 2007. Targeted ablation of osteocytes induces osteoporosis with defective mechanotransduction. Cell Metab. 5, 464–475.
Thomsen, J.S., Christensen, L.L., Vegger, J.B., Nyengaard, J.R., Bruel, A., 2012. Loss of bone strength is dependent on skeletal site in disuse osteoporosis in rats. Calcif. Tissue Int. 90, 294–306.
van Hove, R.P., Nolte, P.A., Vatsa, A., Semeins, C.M., Salmon, P.L., Smit, T.H., Klein-Nulend, J., 2009. Osteocyte morphology in human tibiae of different bone pathologies with different bone mineral density—is there a role for mechanosensing? Bone 45, 321–329.
van Oers, R.F., Wang, H., Bacabac, R.G., 2015. Osteocyte shape and mechanical loading. Curr. Osteoporos. Rep. 13, 61–66.
Vashishth, D., Gibson, G.J., Fyhrie, D.P., 2005. Sexual dimorphism and age dependence of osteocyte lacunar density for human vertebral cancellous bone. Anatomical Record Part a-Discoveries in Molecular Cellular and Evolutionary Biology. 282A pp. 157–162.
Vogel, H.G., 1979. Influence of maturation and aging on mechanical and biochemical parameters of rat bone. Gerontology 25, 16–23.
Wronski, T.J., Dann, L.M., Scott, K.S., Cintron, M., 1989. Long-term effects of ovariectomy and aging on the rat skeleton. Calcif. Tissue Int. 45, 360–366.
Yao, W., Cheng, Z.Q., Koester, K.J., Ager, J.W., Balooch, M., Pham, A., Chefo, S., Busse, C., Ritchie, R.O., Lane, N.E., 2007. The degree of bone mineralization is maintained with single intravenous bisphosphonates in aged estrogen-deficient rats and is a strong predictor of bone strength. Bone 41, 804–812.
Zhang, R., Gong, H., Zhu, D., Ma, R., Fang, J., Fan, Y., 2015. Multi-level femoral morphology and mechanical properties of rats of different ages. Bone 76, 76–87.
Zimmermann, E.A., Ritchie, R.O., 2015. Bone as a structural material. Adv. Healthcare Mater. 4, 1287–1304.